

Macrocyclic ligands bearing two 3-(Hydroxy)-2-pyridinone moieties as side-arms. Conformational studies, synthesis, crystal structure, and alkali and alkaline earth complex formation

Gianluca Ambrosi,^a Paolo Dapporto,^b Mauro Formica,^a Vieri Fusi,^{*a} Luca Giorgi,^a Annalisa Guerri,^b Simone Lucarini,^c Mauro Micheloni,^{*a} Paola Paoli,^b Roberto Pontellini,^a Patrizia Rossi^b and Giovanni Zappia^c

^a Institute of Chemical Sciences, University of Urbino, P.za Rinascimento 6, I-61029 Urbino, Italy. E-mail: vieri@chim.uniurb.it

^b Department of Energy Engineering 'Sergio Stecco', University of Florence, Via S. Marta 3, I-50139 Florence, Italy

^c Institute of Pharmaceutical Chemistry, University of Urbino, P.za Rinascimento 6, I-61029 Urbino, Italy

Received (in Durham, UK) 21st July 2004, Accepted 17th August 2004
First published as an Advance Article on the web 18th October 2004

The synthesis and characterization of the new tetraazamacrocycle 4(N),10(N)-bis[2-(3-hydroxy-2-oxo-2H-pyridin-1-yl)ethyl]-1,7-dimethyl-1,4,7,10-tetraazacyclododecane (**L1**) is reported. **L1** shows two 3-(hydroxy)-1-(carbonylmethylen)-2(1H)-pyridinone (HPO) moieties linked to the macrocyclic base 4,7-dimethyl-1,4,7,10-tetraazacyclododecane, as side-arms. The acid–base and coordination properties towards alkali, alkaline earth ions of **L1** together with those of the structurally similar ligand 4-(N),10-(N)-bis[2-(3-hydroxy-2-oxo-2H-pyridin-1-yl)acetamido]-1,7-dimethyl-1,4,7,10-tetraazacyclododecane (**L2**) are reported. **L2** binds all the metal ions investigated forming stable mono-nuclear complexes, while **L1** binds only some alkaline earth ions with stability constants lower than those of **L2**. Both compounds show selectivity towards the Mg(II) ion with respect to the alkaline earth series. The binding area is formed by the four converging oxygen atoms of the two HPO groups. **L2** appears to be a more efficient ligand in the coordination of hard metal ions because the two HPO binding groups are forced by the macrocyclic skeleton to stay on the same part of the macrocyclic ring, while this conformation is unfavourable for **L1**. These data are supported by molecular dynamics (MD) simulations performed on both ligands and by the crystal structure of the [H₂L1](ClO₄)₂ species which shows the two side-arms displaced opposite to the macrocyclic ring. The effects of pH and metal ion coordination on the UV-Vis absorption and fluorescence emission properties of both ligands were investigated, highlighting that the optical properties changes in acid–base reactions as well as in the coordination of metal ions.

Introduction

The properties of multifunctional ligands suitable to interact with guests having different charge and nature are a challenging field of study. For this purpose, macrocyclic molecules show countless possibilities; these ligands and their complexes are used as selective binders of metal ions, simple models for biologically relevant systems, hosts for charged and uncharged guests, catalysts, NMR contrast agents, photochemical devices, selective extractants, analytical reagents, *etc.*^{1–8}

A synthetic strategy which can widen the potential applications of macrocycles involves attaching side-arms on the macrocyclic skeleton. In this way it is possible to combine different chemical properties, exploiting the binding properties of both macrocyclic and molecular fragments connected as side-arms.^{9–12} Molecules containing many 3-hydroxy-2(1H)-pyridinone (HPO) groups in their skeleton are chelating agents that have shown peculiar binding and sequestering properties towards metal cations with a high charge.^{13–16} Moreover, the HPO group shows atoms able to form hydrogen bonds with other species. This capability can be pH-modulated in solution, producing donor or acceptor sites of hydrogen bonds.¹⁷ Recently, we reported the coordination properties of ligand **L2** (Fig. 1) towards ammonium guests in which two attached HPO

moieties had been driven to cooperate in the binding of organic guests by the macrocyclic skeleton of the 1,4-dimethyl-1,4,7,10-tetraazacyclododecane (Me₂[12]aneN₄).^{17a}

Molecular modeling highlighted the fundamental role of the two N–C=O groups, which link each HPO moiety to the twelve membered ring, in stiffening and preorganizing the host. In fact, the two amide moieties force the two side arms to occupy the same region with respect to the macrocycle leading to the formation of an electron rich area able to recognize, *via* hydrogen-bond, guests difficult to bind in aqueous solution, such as ammonium cations. These results encouraged us to extend the study with **L2** addressing the binding of hard metal cations, which are also difficult to bind in aqueous solution; this investigation was part of the present study.

However a question still remains open, that is, how much does the binding ability of **L2** depend on the nature of the link between the HPO side arms and the macrocyclic framework, and therefore on the rigid topology of the host? Or does the chelating nature of HPO suffice to account for the binding properties of **L2**? By exploiting the molecular modelling tools we decided to focus on this aspect by studying **L1** (Fig. 1) where the linkage between each HPO group and the Me₂[12]aneN₄ moiety occurs by means of an amine N–CH₂ function. The results obtained reveal that the hosts differ both

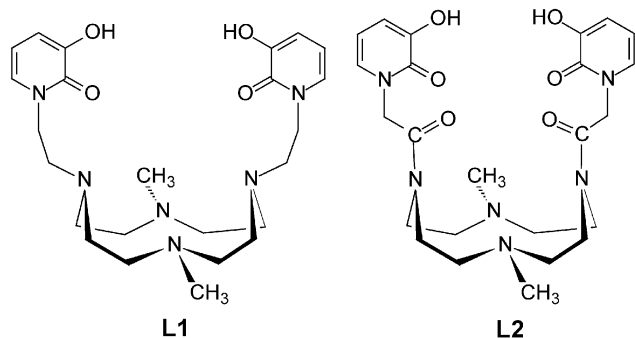


Fig. 1 Schematic draws of ligands **L1** and **L2**.

in their overall molecular shape and in terms of flexibility. On this basis **L1** should be the ideal probe to test the interplay between the host topology and the nature of the coordinating moiety (HPO) in binding small charged species such as hard metal cations. Thus we decided to proceed with the synthesis of **L1** (here reported) and the study of its acid–base and binding properties which were compared with those of **L2**.

The binding efficiency of **L1** and **L2** was tested on the families of alkali and alkaline earth ions, which play a relevant role in biological systems and in medicine. A detailed understanding of the modes of complexation of these cations is therefore of great importance for selection of optimal ligands for example, to produce better sensors.

Complexation equilibria in aqueous solution with both ligands were studied by potentiometric and NMR experiments. Given the optical properties shown by the HPO fragment, it was hypothesized that both ligands could be attractive as chemosensors, *i.e.*, as molecular systems capable of binding guests and at the same time signalling the interaction. Thus the fluorescence and UV-Vis features of **L1** and **L2** were monitored with and without the metal ions.

Results and discussion

Preliminary modeling studies

Ligand **L1** appears to be an ideal candidate to assess, with respect to **L2**, how much the rigidity of the host determines its binding properties, given that the stiffness of the latter has to be ascribed to its amide functions.^{17a} The modeling approach, devised to gain information on the molecular topology, based on the conformational degree of freedom and dynamics of **L1** with respect to **L2**, had as the ultimate goal the evaluation of the coordinating ability of both ligands towards the hard metal ions (*vide infra*). Thus at first our attention was devoted to the mono-negative species of **L1** (and **L2** for comparative purposes) whose conformational space was investigated by means of molecular dynamics runs performed *in vacuo*, to compare the rigidity of the hosts. Two main reasons led us to choose $H_{-1}L^{-}$ as the chief species for our preliminary tests:

(i) the electrostatic nature of the metal ion–ligand interaction which favours overall negatively charged ligands (*i.e.* $H_{-1}L^{-}$ or $H_{-2}L^{2-}$)

(ii) the fact that in the $H_{-1}L^{2-}$ species, fully formed at pH = 10, the two HPO groups are both present in solution in their deprotonated form.^{17a}

Two different starting conformations were considered for each anion ($H_{-1}L^{-}$): the first one (U shaped) featuring the two side arms staying on the same part with respect to the $Me_2[12]aneN_4$ moiety (Fig. 2a), almost facing each other, while in the other one (S in shape) the two HPO arms are pointing in the opposite direction with respect to the mean plane containing the twelve membered ring (Fig. 2b). As expected, $H_{-1}L^{2-}$ appears quite rigid and no U \rightarrow S conversion takes place, conformations with the two side arms almost facing (U) are the

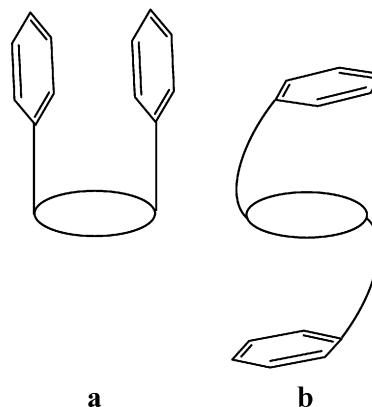


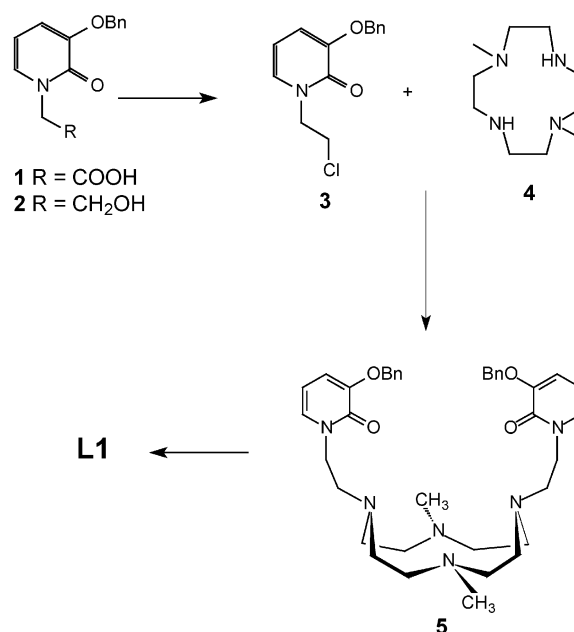
Fig. 2 Proposed models for: (a) the U shaped and (b) the S shaped anion $H_{-1}L^{-}$.

preferred ones (~ 20 kcal mol⁻¹ more stable). Conversely $H_{-1}L^{-}$ was shown to be significantly flexible, allowing the U \rightarrow S conversion, being the preferred conformation the S shaped. Thus not only is the dynamics behaviour of **L1** and **L2** appreciably different in terms of flexibility, the hosts also differ in their preferred molecular topology.

Synthesis

Scheme 1 outlines the synthesis of the new multidentate ligand **L1**, which was based on the coupling of the alkyl-halide reagent **3** with the 1,7-dimethyl-1,4,7,10-tetraazacyclododecane **4**, followed by the removal of the hydroxyl function protection.

Reduction of the known carboxylic acid **1** with BH_3/THF afforded the corresponding alcohol **2**^{15b} in 90% yield; **2** was treated with $TsCl/Et_3N$ to produce the chloride derivative **3** in high yield (86%). Treatment of **3** (2 equiv.) with the 1,7-dimethyl-1,4,7,10-tetraazacyclododecane **4** (1 equiv.) in dry CH_3CN in the presence of K_2CO_3 (4 equiv.) gave the protected ligand **5** (40%). Finally, hydrogenation of **5** in the presence of 10% Pd/C afforded the free ligand **L1** in almost quantitative yield. The compound was further purified as the diperchlorate salt.



Scheme 1 Synthesis of **L1**.

Solid state structure of $[\text{H}_2\text{L1}] \cdot (\text{ClO}_4)_2$

The diprotonated ligand possesses a symmetry centre; as a consequence, the unit cell contains one $(\text{H}_2\text{L1})^{2+}$ cation and two symmetry-related perchlorate anions (see Fig. 3).

The collected crystallographic data did not allow location of the position of the acidic hydrogen atoms in the Fourier difference map, however they can be easily localized by the following considerations:

(1) the acidic hydrogens must be bound to two nitrogen atoms of the $(\text{Me}_2[12]\text{aneN}_4)$.

(2) due to the presence of the symmetry centre they are bound to opposite nitrogen atoms, *i.e.* N(2), N(2)' or N(3), N(3)' ($' = -x + 1, -y, -z$).

Steric hindrance allows us to exclude the first possibility, in fact if the two protonation hydrogens were bound to N(2) and N(2)' they would be too near to the hydrogen atom H(11a) bound to the carbon atom C(11). As a consequence the two acidic hydrogens must be bound to N(3) and N(3)'. The short distance between N(3) and O(1) [2.72(1) Å] nicely supports our hypothesis. Finally this latter interaction could explain the overall shape taken by the ligand (*vide infra*).

The hydrogen atom bound to O(2) was not found in the Fourier difference map. However given the short distance between O(2) and perchlorate oxygen atom O(4) [2.847(9) Å], the presence of a strong hydrogen bond¹⁸ between the hydrogen bound to O(2) and the oxygen atom O(4) may be inferred. Due to the presence of these interaction between $[\text{H}_2\text{L1}]^{2+}$ and the perchlorate anions, the crystal lattice is made up of ionic couples.

Thanks to the *syn*-clinal¹⁹ or *gauche* conformation shown by the dihedral angles governing the orientation of the side arms, each pyridinone moiety forms a sort of top on the opposite sides of the 12-membered ring. As a consequence, the plane containing the pyridinone and that defined by the twelve atoms of the macrocycle form an angle of 35.3(3)°. The resulting overall shape of the cation strictly resembles that outlined by the MD simulations, and therefore appears to be a peculiar feature of this host, irrespective of the degree of protonation (namely, $\text{H}_{-1}\text{L1}^-$ vs. $\text{H}_2\text{L1}^{2+}$).

Given the sequence of the dihedral angles, the twelve-membered ring has the usual [3333] C corners conformation,²⁰ which, however, deserves some additional comment. In fact,

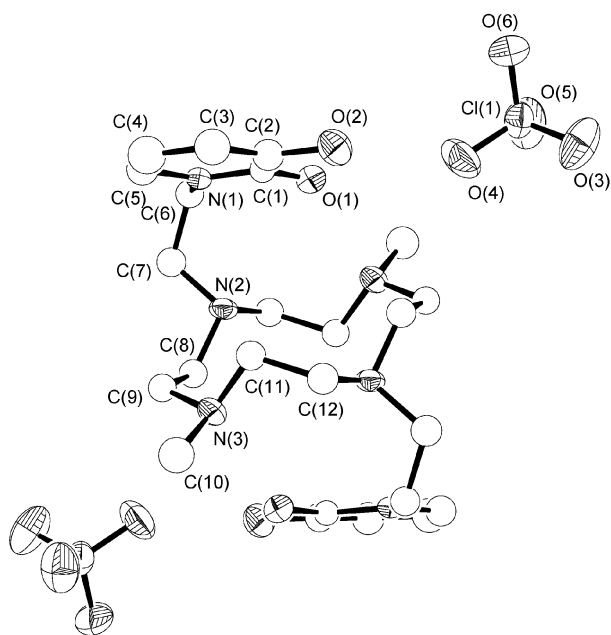


Fig. 3 ORTEP view of the diprotonated ligand together with the interacting perchlorate anions. Ellipsoids are drawn at 40% probability.

a careful examination of analogous structures deposited in the Cambridge Structural Database (CSD, v 5.25)²¹ showed in all the [3333] diprotonated rings that the four N–X hexocyclic bonds have the same orientation (namely “up”) with respect to the best plane through the macrocycle. In each species the values of the four distances between the adjacent nitrogen atoms are very similar and not greater than 3.0 Å. As a consequence the *trans*-diprotonated cation is stabilised by the N–H···N interactions occurring within the ring cavity.²² The $[\text{H}_2\text{L1}]^{2+}$ cation is the first example of an up-up-down-down orientation of the hexocyclic carbon atoms on N(2) and N(3) and their symmetry-related counterpart, with respect to the flattened twelve-membered ring. This orientation for the four nitrogen substituents implies that the number of potential *intra*-annular stabilising H-bond interactions is halved with respect to the usual “all up” disposition of the N–X bonds. In addition the distances between adjacent nitrogen atoms are significantly larger than those observed for the usual [3333] C corners conformation (3.19 and 3.28 Å, for the up-up and up-down pairs, respectively). In our case we can hypothesized that the stabilisation of the biprotonated species is achieved by a hydrogen bond involving the oxygen atom O(1) of the pyridinone moiety [O(1)···N(3)' = 2.72(1) Å, $' = -x + 1, -y, -z$].

Solution studies

Basicity

Table 1 summarizes the basicity constants of **L1** potentiometrically determined in 0.15 M NMe_4Cl aqueous solution at 298.1 K; the basicity constants of **L2** are reported for comparison. The neutral species **L1** behaves as a triprotic base and as a monoprotic acid under the experimental conditions used. As shown in Table 1, it can be present in solution as anionic species $\text{H}_{-1}\text{L1}^-$ indicating the permanence of one acidic hydrogen on the ligand at least at pH lower than 11. In fact, taking into account that each HPO group shows an acidic proton, the $\text{H}_{-2}\text{L1}^{2-}$ species could theoretically be achieved in alkaline solution. This was demonstrated by the basicity behavior of **L2** (see Table 1) in which the species $\text{H}_{-2}\text{L2}^{2-}$, which has lost all of the acidic hydrogen atoms, was detected. In other words, $\text{H}_{-2}\text{L1}^{2-}$ is a stronger base than the same species of **L2**, and it was not possible to evaluate its protonation constant, under the experimental conditions used. This is probably due to the higher number of protonation sites in **L1**; in addition, MD simulations pointed out that, thanks to their flexibility, the HPO side arms stabilize the acidic proton in $\text{H}_{-1}\text{L1}^-$ by N–H···O interactions (the H···O distance ranges from 1.61 to 2.88 Å (mean value 1.86 Å)).

Analysis of the protonation constants starting from the anionic species $\text{H}_{-1}\text{L1}^-$ revealed that **L1** behaves as a rather strong base in the addition of three protons to the $\text{H}_{-1}\text{L1}^-$ species, with protonation constant values ranging from 9.70 to 7.74 logarithmic units, but with a sharp decrease in the last

Table 1 Logarithm of the protonation constants of **L1** and **L2** determined by means of potentiometric measurements in 0.15 M NMe_4Cl aqueous solutions at 298.1 K

Reaction	log <i>K</i>	
	L1	L2
$\text{H}_{-2}\text{L}^{2-} + \text{H}^+ = \text{H}_{-1}\text{L}^-$	> 12	10.79(1) ^b
$\text{H}_{-1}\text{L}^- + \text{H}^+ = \text{L}$	9.70(1) ^a	9.08(1)
$\text{L} + \text{H}^+ = \text{HL}^+$	8.39(1)	8.33(1)
$\text{HL}^+ + \text{H}^+ = \text{H}_2\text{L}^{2+}$	7.74(1)	1.86(2)
$\text{H}_2\text{L}^{2+} + \text{H}^+ = \text{H}_3\text{L}^{3+}$	2.30(3)	

^a Values in parentheses are the standard deviations on the last significant figure. ^b From ref. 17a.

proton addition ($\log K = 2.30$). This trend suggests an easy availability of the protonation sites up to the HLI^+ species, in agreement with the topology of the ligand. For these reasons, the four acidic protons in the H_2LI^{2+} species are probably located far from each other, two on each HPO moiety and the other two on non-contiguous amine groups of the macrocyclic base in a disposition closely resembling that inferred from the crystal structure of this species (see Fig. 3). The undetectable value of the first constant and the value of the second protonation constant, which was similar to that found for the free tetraaza-macrocyclic base and higher than that of L2 ,^{17a,23} suggest an involvement of the amine functions of the macrocyclic base in both protonation steps. In the other two steps, the deprotonated HPO groups should instead be involved in the protonation processes.

Spectroscopic studies were performed on L1 to ascertain which of the protonation steps the HPO moieties are involved in. To this aim, absorption UV-Vis and emission fluorescence spectra were recorded for L1 at different pH values. Given its response to light stimuli, the HPO group can be considered a suitable chromophore not only in absorbance but also in fluorescence.

The UV-Vis spectra show different features in acid or basic pH fields and the spectra obtained are similar to those of L2 .^{17a} At pH = 2, where the H_3L^{3+} species is prevalent in solution (see Fig. 4a), two λ_{max} at 232 ($\epsilon = 9600 \text{ cm}^{-1}\text{mol}^{-1}\text{dm}^3$) and 301 nm ($\epsilon = 13700 \text{ cm}^{-1}\text{mol}^{-1}\text{dm}^3$) can be observed; these data are preserved also at pH less than 2. At pH = 12, where the H_-1L^- species is prevalent in solution, two new bands with λ_{max} at 258 ($\epsilon = 10800 \text{ cm}^{-1}\text{mol}^{-1}\text{dm}^3$) and 313 nm ($\epsilon = 16700 \text{ cm}^{-1}\text{mol}^{-1}\text{dm}^3$) appear (see Fig. 4a). No further changes were observed in the spectra at more strongly alkaline pH.

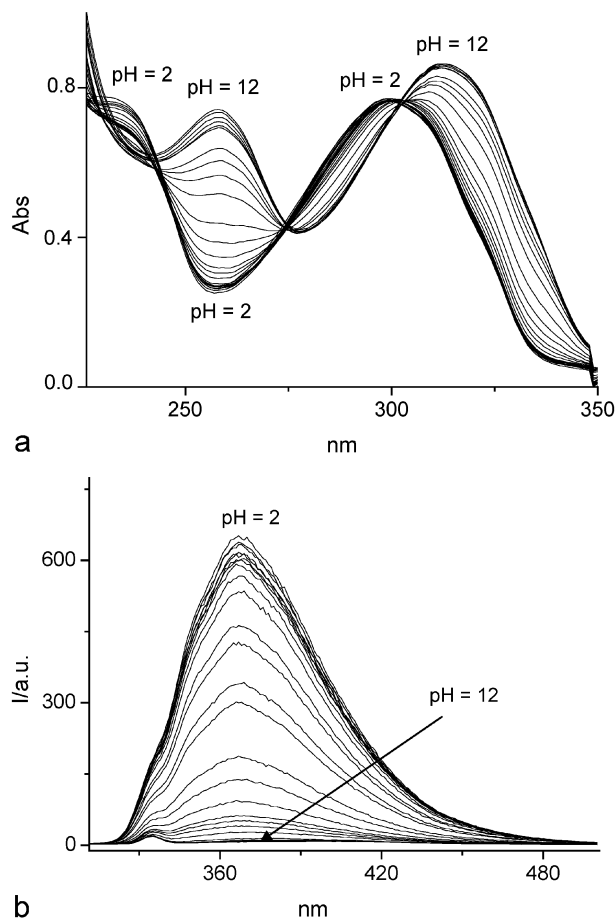


Fig. 4 Absorption spectra (a), and fluorescence emission spectra (b) of L1 at different pH values ($[\text{L1}] = 6.8 \times 10^{-5} \text{ M}$ (a) and $5 \times 10^{-6} \text{ M}$ (b); $\lambda_{\text{exc}} = 301 \text{ nm}$, $\lambda_{\text{em}} = 368 \text{ nm}$).

These different spectral features in the opposite field of pH can be ascribed to the presence in solution of the neutral form of the pyridinone moieties at low pH values and of their deprotonated form at alkaline pH values.¹⁷ The bands at higher energy are attributed to the $\pi \rightarrow \pi^*$ while those at lower energy to the $n \rightarrow \pi^*$ electronic transitions of protonated or deprotonated HPO, for both spectra.²⁴

By monitoring the spectra from acid to basic pH and plotting the absorbance of one of the λ_{max} ($\lambda = 258 \text{ nm}$ in Fig. 5a, square blocks) versus pH, it is possible to determine during which deprotonation steps the HPO groups lose the acidic protons by coupling the trend of the absorbance with the distribution diagram of the species obtained by potentiometric measurements (lines in Fig. 5). Absorbance at 258 nm was lowest at pH < 6, and increases at higher pH, reaching a maximum value at pH = 10. Considering the distribution diagram of the species, absorbance increases upon the appearance of the HLI^+ species and continues to increase in the presence of the neutral species L , reaching a plateau at approximately pH > 10. Taking into account that the change in absorbance is due to the deprotonation of the HPO groups, this profile can be attributed to the deprotonation of one chromophore which occurs in the formation of the HLI^+ species and to a second deprotonation of the other HPO which takes place in the formation of the neutral L species (see Scheme 2). For these reasons, the acidic proton in the H_-1LI^- species must be located on the macrocyclic base as above suggested. Similar behavior had also been found for compound L2 , and is reported for clarity in Fig. 5b ($\lambda = 258 \text{ nm}$, square blocks). In this case, the deprotonation of HPO occurs in the formation of neutral L2 and mononegative $\text{H}_-1\text{L2}^-$ species.

Excitation of acid solutions of both L1 and L2 compounds ($\lambda_{\text{exc}} = 301 \text{ nm}$), gave rise to a fluorescence emission band ($\lambda_{\text{em}} = 368 \text{ nm}$) attributed to the HPO fluorophore; similar spectra were recorded for both compounds. The intensity

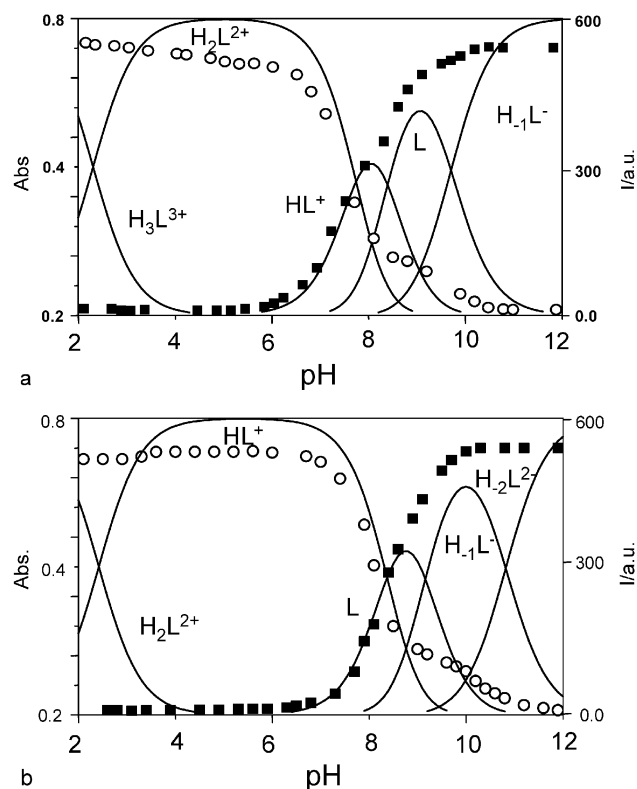
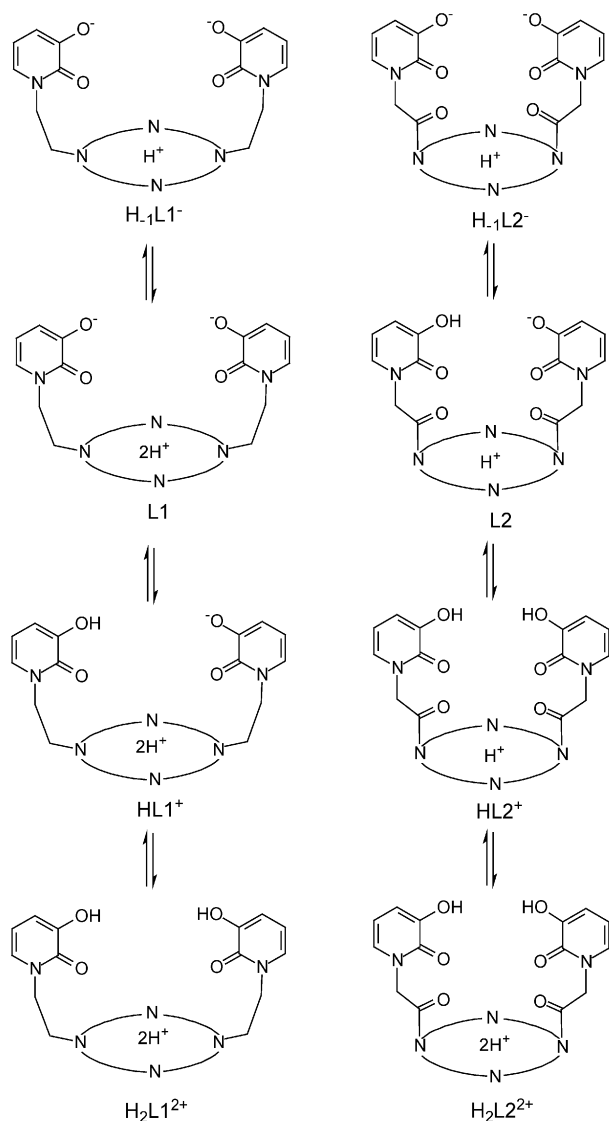


Fig. 5 Fluorescence emission (\circ) ($[\text{L}] = 5.0 \times 10^{-6} \text{ M}$), absorption titration (\blacksquare) ($[\text{L}] = 6.8 \times 10^{-5} \text{ M}$), and distribution curves of the species (line) for $\text{L} = \text{L1}$ (a) and $\text{L} = \text{L2}$ (b) in aqueous solution at 298.1 K in 0.15 M NMe_4Cl ; $\lambda_{\text{exc}} = 301 \text{ nm}$, $\lambda_{\text{em}} = 368 \text{ nm}$, absorbance at $\lambda = 258 \text{ nm}$.



Scheme 2 Acidic hydrogen atoms location in the differently protonated species of **L1** and **L2**.

of the fluorescence emission spectra of the two compounds is highly dependent on the protonation state of the HPO groups (see Fig. 4b); however, the shape and position of the spectra is substantially independent of pH in both ligands. Analogous behavior was observed for similar fluorescent groups, suggest-

ing that the fluorescence intensity changes reflect only the ground states acid–base equilibrium; thus, no indication of excited state proton transfer reaction was found.²⁴

The trend of fluorescence emission at 368 nm *versus* pH ($\lambda_{\text{exc}} = 301$ nm) is reported in Fig. 5a and 5b for **L1** and **L2**, respectively. In the emission spectra at 368 nm *versus* pH, a quenching of the emission can be observed at alkaline pH values for both **L1** and **L2** (Fig. 5a and 5b, circle blocks). Taking into account the absorption data, this behavior can be ascribed to the deprotonation of the HPO groups, the effect of which is to dramatically decrease the emission intensity of HPO. The first deprotonation of one of the HPO moieties also affects the other group, giving rise to a significant drop in emission for both compounds. This occurs during the deprotonation of $\text{H}_2\text{L1}^{2+}$ and of HL2^+ species yielding the HL1^+ and **L2** species, respectively (see Fig. 5a and 5b). A drop in the emission is also observed for the subsequent deprotonation of these species suggesting, as above hypothesized, the deprotonation of the other HPO group.

In conclusion, ligands **L1** and **L2** behave as chemosensors for H^+ , giving rise to the greatest fluorescence when HPO is in its neutral form; the emission is quenched when the group loses its acidic proton. The presence of amine functions, which in many chemosensors can affect the fluorescence of the sensing group, in this case seems to be unimportant.

Coordination of metal ions

The coordination properties of **L1** and **L2** were studied in 0.15 M NMe_4Cl aqueous solution at 298.1 K. The stability constants for the equilibrium reactions of the two macrocycles with Li^+ , Na^+ , K^+ , Cs^+ and Mg^{2+} , Ca^{2+} , Sr^{2+} and Ba^{2+} were potentiometrically determined and are reported in Table 2. Both ligands form only mononuclear species with the metal ions examined; the main difference between **L1** and **L2** is that the latter binds both alkali and alkaline earth metal ions, while **L1** binds only some of the alkaline earth metal ions. In particular, **L2** binds Li^+ , Na^+ and K^+ with the anionic $\text{H}_{-2}\text{L}^{2-}$ and H_{-1}L^- species while Cs^+ is not bound; the values of the addition constants are similar for all the three metals. The absence of interaction with the bigger Cs^+ suggests that the binding zone is barely adaptable to the dimensions of the cations. Considering that the coordination is essentially due to non-covalent interactions and taking into account that under these experimental conditions, the macrocyclic base of **L2** with only two amine donor groups displaced far from each other cannot bind hard metal ions, the HPO moieties should be mainly involved in the binding of the metal cations. Thus **L2**,

Table 2 Logarithms of the equilibrium constants (LogK) determined in 0.15 M NMe_4Cl at 298.1 K for the complexation reactions of **L1** and **L2** with alkali and alkaline earth metal ions

Reaction	L = L1			
	Mg^{2+}	Ca^{2+}	Sr^{2+}	Ba^{2+}
$\text{M}^{2+} + \text{H}_{-1}\text{L}^- = \text{MH}_{-1}\text{L} + \text{H}^+$	-6.28(4) ^a	—	—	—
$\text{M}^{2+} + \text{H}_{-1}\text{L}^- = \text{MH}_{-1}\text{L}^+$	5.22(2)	3.18(3)	2.57(1)	—
Reaction	L = L2			
	Mg^{2+}	Ca^{2+}	Sr^{2+}	Ba^{2+}
$\text{M}^{2+} + \text{H}_{-2}\text{L}^{2-} = \text{MH}_{-2}\text{L}$	7.08(2)	5.88(2)	4.30(3)	3.96(4)
$\text{M}^{2+} + \text{H}_{-1}\text{L}^- = \text{MH}_{-1}\text{L}^+$	6.15(1)	5.36(1)	3.81(3)	3.42(2)
Reaction	Li^+	Na^+	K^+	
$\text{M}^+ + \text{H}_{-2}\text{L}^{2-} = \text{MH}_{-2}\text{L}^-$	2.39(4)	2.66(4)	2.15(5)	
$\text{M}^+ + \text{H}_{-1}\text{L}^- = \text{MH}_{-1}\text{L}$	1.67(3)	2.15(5)	1.51(5)	

^a Values in parentheses are the standard deviations on the last significant figure

whose side arms are already preorganised by the macrocyclic skeleton (the two amide groups stiffen the whole molecule which prefers a U shape, MD data), easily binds the alkali metal cation. However, the four oxygen atoms provided by the HPO moieties converge to shape a quite rigid binding area, as already demonstrated in ammonium cation recognition.^{17a} On the contrary, the preferred S shape of **L1**, (MD data) featuring the two side arms in opposite direction with respect to the macrocycle, is very unfavorable for the uptake of the alkali metal cations.

As already stated, both ligands bind alkaline earth metal ions but, while **L2** binds all the metal ions investigated, **L1** does not bind Ba^{2+} (see Table 2). **L2** binds the metals with its dianionic species H_2L^{2-} ; moreover, **L1** binds only Mg^{2+} with this species, producing the removal of the last acidic proton in the presence of this alkaline earth ion. On the contrary, the anion H_1L^- is a coordinating species for both ligands.

Analysis of the stability constants of **L2** revealed a trend of the values with a peak of selectivity towards Mg^{2+} with both active binding species. The addition of Mg^{2+} exhibits a very high values of $\text{Log } K = 7.08$ and 6.15 to the H_2L^{2-} and H_1L^{2-} species, respectively. The affinity values for the addition of each M^{2+} to the anionic H_1L^- species are similar to those for the addition to the bi-negative H_2L^{2-} species, denoting that the acidic proton does not perturb the coordination of the metal ion; thus, we can safely assume that it is located far from the binding area, *i.e.* in the macrocyclic base bound to an amine group. The value of the constants, which decreases when the dimensions of the cation increase, once again supports the hypothesis that the two HPO shape a rigid preorganized binding area formed by the four oxygen atoms of the HPO groups in both H_2L^{2-} and H_1L^- species. Finally, **L2** shows higher stability constants with the alkaline earth than with the alkali metal ion as expected when the coordination is mainly due to electrostatic ligand–metal interactions.

Taking into account the addition of M^{2+} to the H_1L^- species, the value of the stability constants for the corresponding $[\text{MH}_1\text{L}]^+$ complexes once again decreases when the size of the coordinated metal ions increases, reaching a point at which it is no longer able to bind the bigger Ba^{2+} .

Comparison of the values of the addition constant of each M^{2+} to the H_1L^- species for both ligands revealed that **L2** always has higher stability constants and thus has a greater capability to bind hard metal ions. This behavior, as illustrated above, can be ascribed to the higher level of preorganization of the two HPO groups in **L2** as compared to **L1**; in the case of **L1**, this preorganization is sufficient to bind the bi-positively charged alkaline earth Mg^{2+} , Ca^{2+} and Sr^{2+} but insufficient to bind the mono-charged alkali metal ions.

Spectrophotometric experiments. UV/Vis spectra were recorded in the field of pH in which the complexed species of **L1** and **L2** are present and compared with those of the H_1L^- and H_2L^{2-} species recorded under the same experimental conditions. No marked differences in absorbance or in λ_{max} were found by comparing the spectra of alkali and alkaline earth complexes, thus indicating that the complexation of the metal does not strongly perturb the optical properties of the chromophores and thus the electronic states.

Even though the spectral profiles of the complexed species are similar to those of H_1L^- and H_2L^{2-} species in the absence of the metal ions, they are quite different when comparing the spectra of the M/L system with that of L at the same pH values. This mainly occurs in the case of Mg/L2 system, which shows the highest stability constants. The same observations were made for the fluorescence emission spectra. These spectral differences are due to the fact that the binding species of the ligands appear at lower pH values in the presence of the metal ions than in the absence of them (see Fig. 6).

In the Mg/L2 system, the main differences were observed at physiological pH (pH = 7.4). At this pH, the percentage of

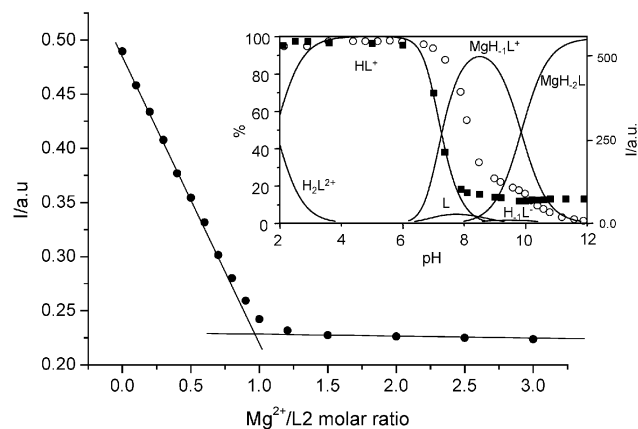


Fig. 6 Variation of the fluorescence emission intensity of **L2** solution ($[\text{L2}] = 5 \times 10^{-6}$ M) at pH = 7.4, as a function of $\text{Mg}^{2+}/\text{L2}$ molar ratio. Inset: distribution curves of the species (line) for the Mg/L2 system in molar ratio 1 : 1; fluorescence emission for the Mg/L2 system (\blacksquare) and for **L2** (\circ) ($[\text{L2}] = 5 \times 10^{-6}$ M) at different pH values in aqueous solution at 298.1 K; $\lambda_{\text{exc}} = 301$ nm, $\lambda_{\text{em}} = 368$ nm, absorbance at $\lambda = 258$ nm.

$[\text{MgH}_1\text{L2}]^+$ species in the system with M/L of 1 : 1 molar ratio is 57%; on the contrary, the binding H_1L^- species is substantially absent at this pH in the absence of Mg^{2+} (see distribution diagram of the species in Figs. 5b and 6). In other words, the presence of magnesium contributes to deprotonate the HPO side-arms by forming the binding species at pH values lower than in the ligand alone. Keeping in mind that the deprotonation of the HPO gives rise to the modifications in the absorption and emission spectral features of the ligands, the spectra at pH = 7.4 have different absorptivity and intensity of emission in the presence of Mg^{2+} even though the emission or absorption spectra of $[\text{MgH}_1\text{L2}]^+$ and H_1L^- species are, for example, quite similar. This difference is more remarkable in the fluorescence emission spectra recorded at pH 7.4. In fact, while the free ligand shows a higher emission at this pH due to the presence of the emitting species HL^- (see Fig. 5b), in the presence of Mg^{2+} there is the formation of the $[\text{MgH}_1\text{L2}]^+$ species; this produces a quenching of the fluorescence because the complexed species is formed by the not emitting H_1L^- species. For this reason, the relative intensity of the emission in the presence of Mg^{2+} is lower at pH 7.4 than that of the free ligand. This reduction can also be reported as Job plot (Fig. 6) supporting the formation of only adducts Mg/L2 of 1 : 1 stoichiometry at this pH. These results suggest a possible application of **L2** for use as chemosensor for detecting and quantifying Mg^{2+} in physiological solution.

NMR experiments. ^1H and ^{13}C NMR experiments were performed for the M(n)/L2 system in D_2O solution. The ^1H NMR spectra of the HPO resonances of the Mg/L2 system in 1 : 1 molar ratio were recorded at pH = 8.5, where the $[\text{MgH}_1\text{L2}]^+$ species is prevalent in solution (see Fig. 6), is reported in Fig. 7 together with that of **L2** in absence of Mg^{2+} recorded at the same pH value. Comparing the form and the chemical shift of the spectra some changes are observable; the resonances of the HPO groups become broad in the presence of the metal ion, moreover, the resonances shift with respect to those of the free ligand. In particular, the two doublets attributed to the hydrogen atoms in 4- and 6-position (see Fig. 7) shift upfield while the resonance of those in 5-position shifts downfield. The upfield shift can be explained by a deprotonation of the HPO groups due to the formation of the $[\text{MgH}_1\text{L2}]^+$ species; the downfield shift can be attributed to an involvement of the amide oxygen atom of each HPO group in Mg^{2+} stabilization. The latter hypothesis is supported by the consideration that this resonance, in the absence of Mg^{2+} , did not show a great shift for the several species of **L2** existing in

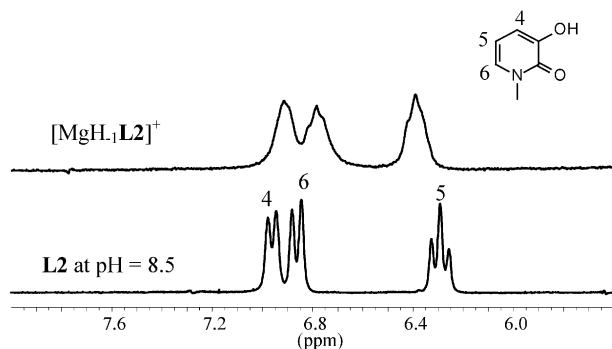


Fig. 7 ^1H NMR spectra of Mg/L2 system of 1 : 1 molar ratio and L2 recorded in aqueous solution at pH = 8.5.

aqueous solution at different pH values.^{17a} The observed changes indicate the coordination of Mg^{2+} by L2 mainly perturbing the HPO groups, thus supporting the hypothesis that the area of L2 in which the M(II) are stabilized is formed by the four oxygen atoms of the HPO groups. Aliphatic resonances resulted quite similar in both systems and thus they were not reported. These data are also supported by those from the ^{13}C NMR experiments. The NMR experiments performed in the presence of the other alkaline earth metal ions gave similar results for both ligands.

Conclusions

The synthesis of the new macrocyclic ligand L1 containing two pyridinone side-arms attached to a tetraaza macrocyclic scaffold is reported. L1 differs from a previously synthesized ligand L2 in its mode of linking the two HPO units to the macrocyclic $\text{Me}_2[12]\text{janeN}_4$ base. While in L2 the two HPO moieties are linked by a rigid amide $\text{N}-\text{C}=\text{O}$ group, in L1 both linkages occur by a more flexible amine $\text{N}-\text{CH}_2$ group. This change affects the acid–base but above all the coordination properties of the two ligands towards hard metal ions. In fact, in aqueous solution L2 binds all the metal ions investigated, with the exception of Cs^+ , and shows a peak of selectivity towards Mg^{2+} . Instead L1 binds only some of the alkaline earth ions examined, while the alkali ions are not bound at all. L1 exhibits lower stability constant values than those of L2 with the same metal ions. In other words, L2 appears to be more preorganized for the coordination of hard metal ions with respect to L1 although the latter shows more coordination sites. These considerations are supported by coordination data in aqueous solution, MD evidences and the crystal structure of the $[\text{H}_2\text{L1}]^{2+}$ species. In the latter species, the two HPO are in opposite position with respect to the mean macrocyclic plane, in contrast to the structure found for the $[\text{HL2}]^+$ cation.^{17a}

Absorbance, fluorescence and NMR experiments support the hypothesis that both HPO groups are involved in the stabilization of all the metal ions coordinated. The fluorescence emission properties of both ligands are ascribed to the HPO groups which are fluorescent as pyridinone or silent, losing the acidic proton, as pyridinonate. Although the complexed species do not strongly affect the spectral behavior of the sensors, an interesting application for the Mg/L2 system can be hypothesized. In fact, a decrease in fluorescence was observed in a solution of L2 in the presence of Mg^{2+} at physiological pH with respect to the free ligand. This suggests that L2 could be used as chemosensor for Mg^{2+} in physiological media to detect and quantify this metal ion in a biological system.

Experimental section

General methods

IR spectra were recorded with a Shimadzu FTIR-8300 spectrometer. Melting points were determined with a Büchi melting

point B 540 apparatus and are uncorrected. EI-MS spectra (70 eV) were recorded with a Fisons Trio 1000 spectrometer; ESI mass spectra were recorded with a ThermoQuest LCQ Duo LC/MS/MS spectrometer. UV absorption spectra were recorded at 298 K with a Varian Cary-100 spectrophotometer equipped with a temperature control unit. Fluorescence spectra were recorded at 298 K with Varian Cary Eclipse spectrofluorimeter. ^1H and ^{13}C NMR spectra were recorded with a Bruker AC-200 instrument, operating at 200.13 and 50.33 MHz, respectively, and equipped with a variable temperature controller. For the spectra recorded in D_2O , the peak positions are reported with respect to HOD (4.75 ppm) for ^1H NMR spectra, while dioxane was used as reference standard in ^{13}C NMR spectra ($\delta = 67.4$ ppm). For the spectra recorded in CDCl_3 , the peak positions are reported with respect to TMS.

Synthesis

Ligand L1 was obtained following the synthetic procedure reported in Scheme 1. 1,4,7,10-tetraazacyclododecane (**4**)²⁵, 4-(N),10-(N)-bis[2-(3-hydroxy-2-oxo-2H-pyridin-1-yl)acetamido]-1,7-dimethyl-1,4,7,10-tetraazacyclododecane (L2)^{17a} and of 3-(benzyloxy)-1-(carboxymethyl)-2-(1H)-pyridinone (**1**)^{15a,17a} were prepared as previously described.

3-Benzyloxy-1-(2-hydroxyethyl)-1H-pyridin-2-one (2)

BH_3 (1 M in THF, 15.44 mmol) was carefully added under nitrogen to a stirred solution of 3-(benzyloxy)-1-(carboxymethyl)-2-(1H)-pyridinone **1** (2 g, 7.72 mmol) in dry THF (15 ml) at 0 °C. The reaction was stirred for 2 h at room temperature, then quenched with ice and extracted with CHCl_3 . Standard work-up afforded the alcohol **2** (1.70 g, 90%) as a white solid which was used without purification; mp 74–75 °C (Lit.^{15b}: 75–76 °C); ^1H and ^{13}C NMR spectra as reported.^{15b}

3-Benzyloxy-1-(2-chloroethyl)-1H-pyridin-2-one (3)

Et_3N (2.55 ml, 18.33 mmol) followed by tosyl chloride (1.46 g, 7.64 mmol) were added to a stirred solution of **2** (1.5 g, 6.11 mmol) in dry CH_2Cl_2 (50 ml) at room temperature. The reaction was stirred overnight, diluted with CH_2Cl_2 (100 ml), washed with 5% aqueous NaHCO_3 (3×50 ml) and brine (1×50 ml). The organic solution was dried over Na_2SO_4 and concentrated *in vacuo*. The yellow oil was purified by flash chromatography (cyclohexane/AcOEt 70 : 30) and to give **3** in 86% yield (1.37 g, 5.22 mmol) as a white solid; mp 84–85 °C; IR (film): 3421, 1650, 1600, 1258 cm^{-1} ; MS m/z (EI): 263 $[\text{M}]^+$, 186 $[\text{M} - \text{Ph}]^+$, 172 $[\text{M} - \text{CH}_2\text{-Ph}]^+$; ^1H NMR: (CDCl_3) δ 7.48–7.24 (m, 5H), 6.97 (dd, $J = 1.7$ Hz, $J = 7.0$ Hz, 1H), 6.69 (dd, $J = 1.5$ Hz, $J = 7.3$ Hz, 1H), 6.05 (t, $J = 7.1$ Hz, 1H), 5.13 (s, 2H), 4.28 (t, $J = 5.7$ Hz, 2H), 3.93 (t, $J = 5.7$ Hz, 2H); ^{13}C NMR: (CDCl_3) δ 158.04, 148.83, 136.14, 130.19, 128.60, 128.06, 127.34, 115.76, 104.39, 70.77, 52.23, 41.93.

4(N),10(N)-Bis[2-(3-Benzyloxy-2-oxo-2H-pyridin-1-yl)ethyl]-1,7-dimethyl-1,4,7,10-tetraazacyclododecane (5)

A solution of 3-benzyloxy-1-(2-chloroethyl)-1H-pyridin-2-one **3** (1.44 g, 5.45 mmol) in dry CH_3CN (50 ml) was added dropwise at 0 °C to a stirred solution of 1,7-dimethyl-1,4,7,10-tetraazacyclododecane **4** (0.55 g, 2.73 mmol) and K_2CO_3 (1.50 g, 10.09 mmol) in dry CH_3CN (50 ml) under nitrogen. The reaction was stirred at room temperature for 48 h, after which the reaction mixture was filtered and the solution concentrated *in vacuo*. The residue was purified by silica gel chromatography (CH_2Cl_2 saturated with NH_3/MeOH 90 : 10) to give the ligand **5** (0.71 g, 40%) as a white solid; mp 116–119 °C dec.; IR (film): 3415, 1648, 1592, 1221 cm^{-1} ; MS m/z (ESI):

677.3 ([M + Na]⁺), 655.3 ([M + 1]⁺); ¹H NMR: (CDCl₃) δ 7.46 – 7.25 (m, 12H), 6.65 (dd, *J* = 1.4 Hz, *J* = 7.3 Hz, 2H), 5.95 (t, *J* = 7.3 Hz, 2H), 5.30 (s, 4H), 3.99 (t, *J* = 5.5 Hz, 4H), 2.71 (t, *J* = 5.5 Hz, 4H), 2.56 (m, 8H), 2.34 (m, 8H), 2.06 (m, 6H); ¹³C NMR: (CDCl₃) δ 158.19, 148.48, 136.48, 131.41, 128.52, 127.91, 127.32, 116.04, 103.77, 70.75, 56.36, 54.71, 53.62, 48.16, 43.68.

4(N),10(N)-Bis[2-(3-Hydroxy-2-oxo-2H-pyridin-1-yl)ethyl]-1,7-dimethyl-1,4,7,10-tetraazacyclododecane (L1)

10% Pd/C (0.15 g) was added to a solution of protected ligand **5** (0.50 g, 0.76 mmol) in dry MeOH (30 ml) and dry CH₂Cl₂ (10 ml) and the mixture was hydrogenated (5 atm.) for 48 h at room temperature. The catalyst was filtered through a Celite pad, and the purple solution was concentrated. The ligand **L1** was obtained in quantitative yield (0.35 g) as purple solid without any further purification; mp: 125–127 °C dec.; MS *m/z* (ESI): 497.3 ([M + Na]⁺), 475.3 ([M + 1]⁺); IR (film): 3455, 1652, 1585, 1232 cm⁻¹; ¹H NMR: (D₂O) δ 6.94 (d, *J* = 6.5 Hz, 2H), 6.58 (d, *J* = 7.5 Hz, 2H), 6.37 (t, *J* = 7.0 Hz, 2H); 4.01 (m, 4H), 3.00–2.50 (m, 26H); ¹³C NMR: (D₂O) δ 163.14, 154.45, 124.69, 119.29, 112.20, 57.06, 56.05, 51.65, 46.76, 43.30.

[H₂L1](ClO₄)₂·**L1** (47.5 mg, 0.1 mmol) was dissolved in H₂O (10 ml) and NaClO₄ (122 mg, 1 mmol) was added to the solution and the pH adjusted to 4 with HClO₄ 0.1 M. Colorless crystals suitable for X-ray analysis formed in a day at room temperature (38 mg, 80%). Anal. for [H₂L1](ClO₄)₂·C₂₄H₄₀Cl₂N₆O₁₂ (675.52): Calcd. C 42.67, H 5.97, N 12.44; Found C 42.6, H 6.0, N 12.3%.

Molecular dynamics (MD) simulation protocol

The species studied were the mono-negative charged anions of **L1** and **L2**, namely: H₋₁L1⁻, and H₋₁L2⁻. The acidic proton in both H₋₁L⁻ anions was located on the macrocycle according to the experimental evidence obtained for **L2**.^{17a}

The MSI software programs InsightII and Discover version 98.0²⁶ were used for all the molecular modelling studies. The force field used was AMBER. MD calculations were performed, *in vacuo* at 300 K and the Verlet leapfrog algorithm, with a time step of 1 fs, was used for integration of equations of motion in all simulations.

Before starting the MD procedures the studied species were optimised until the convergence criterion was met (<0.01 kcal mol⁻¹). For every MD run the system was allowed to equilibrate for 80 ps and then a 800 ps dynamic study was performed (snapshot conformations were saved every ps).

X-ray diffraction

Intensity data concerning the [H₂L1](ClO₄)₂ compound were collected on a MACH3 Nonius diffractometer using a Mo K_α radiation (λ = 0.71069 Å). Cell constants were determined by using 25 reflections. Intensity data were corrected for Lorentz and polarisation effects, an absorption correction was applied once the structure was solved using the Walker and Stuart method.²⁷

The structure was solved by using the package SIR-97²⁸ and subsequently refined on the F² values by the full-matrix least-squares programs SHELXL-97.²⁹

Atomic scattering factors and anomalous dispersion corrections for all the atoms were taken from ref. 30.

Geometrical calculations were performed by PARST97,³¹ and molecular plots were produced by the program ORTEP3.³²

All the non-H atoms were refined anisotropically. All the hydrogen atoms bound to carbon atoms were introduced in calculated positions and refined isotropically with a temperature factor depending on that of the atom to which they are

Table 3 Crystal data and structure refinement parameters for compound [H₂L1]²⁺·(ClO₄⁻)₂

Empirical formula	C ₂₄ H ₄₀ Cl ₂ N ₆ O ₁₂
Formula weight	675.52
Temperature (K)	298
Wavelength (Å)	0.71069
Crystal system, space group	Triclinic, P $\bar{1}$
Unit cell dimensions (Å, °)	<i>a</i> = 8.917(6); α = 90.08(5) <i>b</i> = 9.765(3); β = 111.32(4) <i>c</i> = 10.260(5); γ = 106.14(5)
Volume (Å ³)	794.2(7)
Z, Calculated density (g cm ⁻³)	1, 1.412
Absorption coefficient (mm ⁻¹)	0.273
F(000)	356
Crystal size	0.3 × 0.4 × 0.5 mm
θ range for data collection (°)	2.57 to 25.01
Reflections collected	2791
Refinement method	Full-matrix least-squares on F ²
Data/parameters	1227/141
Final R indices [<i>I</i> > 2σ(<i>I</i>)]	R1 = 0.0927, wR2 = 0.2571
R indices (all data)	R1 = 0.2043, wR2 = 0.3469

bound. The protonation hydrogens and the acidic protons of the HPO moieties were not found in the Fourier synthesis and were not introduced (see “results and discussion” paragraph). Crystallographic data and refinement parameters are reported in Table 3†.

EMF measurements

Equilibrium constants for protonation and complexation reactions with **L1** and **L2** were determined by pH-metric measurements (pH = -log [H⁺]) in 0.15 M NMe₄Cl at 298.1 ± 0.1 K, using the fully automatic equipment that has already been described; the EMF data were acquired with the PASAT computer program.³³ The combined glass electrode was calibrated as a hydrogen concentration probe by titrating known amounts of HCl with CO₂-free NMe₄OH solutions and determining the equivalent point by Gran's method,³⁴ which gives the standard potential *E*^o and the ionic product of water (p*K*_w = 13.83(1) at 298.1 K in 0.15 M NMe₄Cl, *K*_w = [H⁺][OH⁻]). At least three potentiometric titrations were performed for each system in the pH range 2–11, using different molar ratio of M/L ranging from 1 : 1 to 3 : 1. All titrations were treated either as single sets or as separate entities, for each system; no significant variations were found in the values of the determined constants. The HYPERQUAD computer program was used to process the potentiometric data.³⁵

Acknowledgements

The authors thank the Italian Ministero dell'Istruzione dell'Università e della Ricerca (MIUR), PRIN2002 for financial support and CRIST (Centro Interdipartimentale di Cristallografia Strutturale, University of Florence) where the X-ray measurement was carried out.

References

- (a) C. J. Pedersen, *J. Am. Chem. Soc.*, 1967, **89**, 7017; (b) D. J. Cram and J. M. Cram, *Science*, 1984, **183**, 4127; (c) J.-M. Lehn, *Angew. Chem., Int. Ed. Engl.*, 1988, **27**, 89; (d) R. M. Izatt, K. Pawlak and J. S. Bradshaw, *Chem. Rev.*, 1995, **95**, 2529.
- (a) L.-F. Lindoy, *The chemistry of macrocyclic ligand complexes*, Cambridge University Press, Cambridge, 1989; (b) J.-S. Bradshaw,

† CCDC reference number 235708. See <http://www.rsc.org/suppdata/nj/b4/b411165f/> for crystallographic data in .cif or other electronic format.

- Aza-crown Macrocycles*, Wiley, New York, 1993; (c) P. Dietrich, P. Viout and J.-M. Lehn, *Macrocyclic Chemistry*, VCH, Weinheim, 1993.
- 3 (a) N. V. Gerbeleu, V. B. Arion and J. Burgess, *Template synthesis of macrocyclic compounds*, Wiley-VCH, Weinheim, 1999; (b) D. Parker, *Macrocyclic synthesis: a practical approach*, Oxford University Press, Oxford, 1996.
 - 4 G. W. Gokel, *Crown Ethers and Cryptands (Monographs in Supramolecular Chemistry)*, ed. J. F. Stoddart, The Royal Society of Chemistry, Cambridge, 1992.
 - 5 S. Patai, A. Rapport and E. Weber, *Crown Ethers and Analogs*, Wiley, New York, 1998.
 - 6 (a) Y. A. Zoltov, *Macrocyclic compounds in analytical chemistry*, Wiley-Interscience, New York, 1997; (b) M. Formica, V. Fusi, M. Micheloni, R. Pontellini and P. Romani, *Coord. Chem. Rev.*, 1999, **1**; (c) E. Bardazzi, M. Ciampolini, V. Fusi, M. Micheloni, N. Nardi, R. Pontellini and P. Romani, *J. Org. Chem.*, 1999, **64**, 1335; (d) P. Dapporto, M. Formica, V. Fusi, M. Micheloni, P. Paoli, R. Pontellini, P. Romani and P. Rossi, *Inorg. Chem.*, 2000, **39**, 4663.
 - 7 (a) E. Kimura, T. Gotoh, S. Aoki and M. Shiro, *Inorg. Chem.*, 2002, **41**, 3239; (b) C. Bazzicalupi, A. Bencini, E. Berni, A. Bianchi, V. Fedi, V. Fusi, C. Giorgi, P. Paoletti and V. Valtancoli, *Inorg. Chem.*, 1999, **38**, 4115; (c) V. Fusi, A. Llobet, J. Mahia, M. Micheloni, P. Paoli, X. Ribas and P. Rossi, *Eur. J. Inorg. Chem.*, 2002, **4**, 987.
 - 8 (a) *Calixarene in Action*, eds. L. Mandolini and R. Ungaro, Imperial College Press, London, England, 2000; (b) A. Bianchi, K. Bowman-James and E. Garcia-España, *Supramolecular Chemistry of Anions*, Wiley-VCH, New York, 1997.
 - 9 S. Mizukami, T. Nagano, Y. Urano, A. Odani and K. Kikuchi, *J. Am. Chem. Soc.*, 2002, **124**, 3920.
 - 10 (a) P. Dapporto, V. Fusi, M. Micheloni, P. Palma, P. Paoli and R. Pontellini, *Inorg. Chim. Acta*, 1998, **168**, 275–276; (b) C. Bazzicalupi, A. Bencini, A. Bianchi, V. Fedi, V. Fusi, C. Giorgi, P. Paoletti, L. Tei and B. Valtancoli, *J. Chem. Soc., Dalton Trans.*, 1999, 1101.
 - 11 G. Xue, J. S. Bradshaw, N. K. Dalley, P. B. Savage, K. E. Krakowiak, R. M. Izatt, L. Prodi, M. Montalti and N. Zaccaroni, *Tetrahedron*, 2001, **57**, 7623.
 - 12 G. Ambrosi, P. Dapporto, M. Formica, V. Fusi, L. Giorgi, M. Micheloni, P. Paoli, R. Pontellini and P. Rossi, *Chem. Eur. J.*, 2003, **9**, 800.
 - 13 (a) J. Xu, D. W. Whisenhunt, A. C. Veeck, L. C. Uhlir and K. N. Raymond, *Inorg. Chem.*, 2003, **42**, 2665; (b) J. Xu, B. O'Sullivan and K. N. Raymond, *Inorg. Chem.*, 2002, **41**, 6731; (c) C. J. Sunderland, M. Botta, S. Aime and K. N. Raymond, *Inorg. Chem.*, 2001, **40**, 6746; (d) J. Xu, E. Radkov, M. Ziegler and K. N. Raymond, *Inorg. Chem.*, 2001, **39**, 4156.
 - 14 (a) J. Xu, B. Kullgren, P. W. Durbin and K. N. Raymond, *J. Med. Chem.*, 1995, **38**, 2606; (b) M. Meyer, J. R. Telford, S. M. Cohen, D. J. White, J. Xu and K. N. Raymond, *J. Am. Chem. Soc.*, 1997, **119**, 10093; (c) P. W. Durbin, B. Kullgren and K. N. Raymond, *Health Phys.*, 1997, **72**, 865.
 - 15 (a) M. Streater, P. D. Taylor, R. C. Heider and J. Porter, *J. Med. Chem.*, 1990, **33**, 1749; (b) T. N. Lambert, L. Dasaradhi, V. J. Huber and A. S. Gopalan, *J. Org. Chem.*, 1999, **64**, 6097; (c) M. A. Santos, *Coord. Chem. Rev.*, 2002, **228**, 187; (d) V. B. Di Marco, G. G. Bombi, A. Tapparo, A. K. Powell and C. E. Anson, *J. Chem. Soc., Dalton Trans.*, 1999, 2427.
 - 16 (a) G. Xiao, D. Van der Helm, R. C. Hider and J. B. Porter, *J. Med. Chem.*, 1996, **100**, 2345; (b) A. Shanzer, J. Libman, S. Lifson and C. E. Felder, *J. Am. Chem. Soc.*, 1986, **108**, 7609.
 - 17 (a) M. Formica, V. Fusi, L. Giorgi, A. Guerri, S. Lucarini, M. Micheloni, P. Paoli, R. Pontellini, P. Rossi, G. Tarzia and G. Zappia, *New J. Chem.*, 2003, **27**, 1575; (b) B. L. Rai, H. Khodr and R. C. Hider, *Tetrahedron*, 1999, **55**, 1129; (c) J. A. Berson, W. M. Jones and S. L. F. O'Challagan, *J. Am. Chem. Soc.*, 1956, **78**, 622.
 - 18 G. R. Desiraju and T. Steiner, *The weak hydrogen bond*, Oxford University Press, 1999.
 - 19 W. Klyne and V. Prelog, *Experientia*, 1960, **16**, 521.
 - 20 I. Bernal, *Stereochemical and Stereophysical Behaviour of Macrocycles*, Vol. 2, Elsevier, 1987.
 - 21 F. H. Allen, *Acta Cryst.*, 2002, **B58**, 380.
 - 22 P. J. A. Ribeiro-Claro, A. M. Amado, P. M. M. Marques and J. J. C. Teixeira-Dias, *J. Chem. Soc., Perkin Trans.*, 1996, **2**, 1161.
 - 23 R. Hancock, P. Wade and M. Ngwenya, *Inorg. Chem.*, 1990, **29**, 1968.
 - 24 (a) A. Testa, *J. Photochem. Photobiol., A: Chem.*, 1992, **64**, 73; (b) G. Wenska, B. Skalski, Z. Gdaniec, R. W. Adamiak, J. Matulic-Adamic and L. Beigelman, *J. Photochem. Photobiol., A: Chem.*, 2000, **133**, 169–176.
 - 25 M. Ciampolini, P. Dapporto, M. Micheloni, N. Nardi, P. Paoletti and F. Zanobini, *J. Chem. Soc., Dalton Trans.*, 1984, 1357.
 - 26 Biosym/MSI, 9685 Scranton Road, San Diego, CA 92121-3752, USA.
 - 27 N. Walker and D. D. Stuart, *Acta Crystallogr., Sect. A.*, 1983, **39**, 158.
 - 28 A. Altomare, G. L. Cascarano, C. Giacovazzo, A. Guagliardi, M. C. Burla, G. Polidori and M. Camalli, *J. Appl. Cryst.*, 1999, **32**, 115.
 - 29 G. M. Sheldrick, *SHELX 97*, University of Göttingen, Germany, 1997.
 - 30 *International Tables for X-ray Crystallography*, Kynoch Press, Birmingham, UK, Vol. 41974.
 - 31 M. Nardelli, *Comput. Chem.*, 1983, **7**, 95.
 - 32 L. J. Farrugia, *J. Appl. Cryst.*, 1997, **30**, 565.
 - 33 M. Fontanelli and M. Micheloni, *I Spanish-Italian Congr. Thermodynamics of Metal Complexes*, Peñiscola, Univ. of Valencia Spain, June 3–6, 1990, 41.
 - 34 (a) G. Gran, *Analyst*, 1952, **77**, 661; (b) F. J. Rossotti and H. Rossotti, *J. Chem. Educ.*, 1965, **42**, 375.
 - 35 P. Gans, A. Sabatini and A. Vacca, *Talanta*, 1996, **43**, 1739.